Applied and Computational Harmonic Analysis 71 (2024) 101634

Contents lists available at ScienceDirect

Applied and Computational Harmonic Analysis

journal homepage: www.elsevier.com/locate/acha

Full Length Article

New theoretical insights in the decomposition and time-frequency representation of nonstationary signals: The IMFogram algorithm

Antonio Cicone [a,b,c], Wing Suet Li [d,*], Haomin Zhou [d]

[a] DISIM, Università degli Studi dell'Aquila, L'Aquila, Italy
[b] Istituto di Astrofisica e Planetologia Spaziali, INAF, Rome, Italy
[c] Istituto Nazionale di Geofisica e Vulcanologia, Rome, Italy
[d] School of Mathematics, Georgia Institute of Technology, Atlanta, GA, USA

ARTICLE INFO

Communicated by Yang Wang

Keywords:
Time-frequency representations
Nonstationary signals
Empirical Mode Decomposition
Iterative Filtering
Intrinsic Mode Functions

ABSTRACT

The analysis of the time–frequency content of a signal is a classical problem in signal processing, with a broad number of applications in real life. Many different approaches have been developed over the decades, which provide alternative time–frequency representations of a signal each with its advantages and limitations. In this work, following the success of nonlinear methods for the decomposition of signals into intrinsic mode functions (IMFs), we first provide more theoretical insights into the so–called Iterative Filtering decomposition algorithm, proving an energy conservation result for the derived decompositions. Furthermore, we present a new time–frequency representation method based on the IMF decomposition of a signal, which is called IMFogram. We prove theoretical results regarding this method, including its convergence to the spectrogram representation for a certain class of signals, and we present a few examples of applications, comparing results with some of the most well-known approaches available in the literature.

1. Introduction

The study of techniques for the time–frequency (TF) analysis of signals is a long lasting line of research in signal processing which have led over the decades to the development of many new algorithms and approaches, which are nowadays commonly used practically in many fields of research [22]. One of the main goals of these techniques is the derivation of what is called the TF representation (TFR) of a given signal. The TFR is a two-dimensional interpretation of a monodimensional signal, where one dimension relates to time and the other one to frequency. Studying the TFR of a signal allows in many cases to unveil its hidden features, especially the nonstationary ones.

There exist many types of TF analysis algorithms. Most of them belong to either linear or bilinear methods [22]. In linear methods, the signal is studied via inner products with (or correlations with) a pre-assigned basis. The most well-known methods are the windowed Fourier transform [14], and the wavelet transform [17]. However, in all these methods, and related ones, the chosen basis unavoidably leaves its peculiar footprint in the derived TFR, which may badly affect its interpretation when looking for properties of the signal. Moreover, the Heisenberg uncertainty principle limits the maximal achievable resolution of the TF plane

* Corresponding author.
E-mail addresses: antonio.cicone@univaq.it (A. Cicone), li@math.gatech.edu (W.S. Li), hmzhou@math.gatech.edu (H. Zhou).

https://doi.org/10.1016/j.acha.2024.101634
Received 1 July 2022; Received in revised form 13 November 2023; Accepted 19 January 2024

Available online 26 January 2024

due to blurring or smearing out of the TFR. Different choices of the linear transform or basis can produce different trade-offs, but none is ideal [19,53]. In the bilinear methods for TFR, like the Wigner-Ville distribution and, more generally, the Cohen's class or affine class, one can avoid introducing a basis with which the signal is compared or measured. As a consequence, some features can have a crisper and more focused representation in the TF plane with these methods. However, as a side effect, reading the TFR of a multi-component signal becomes more complicated by the presence of interference terms between the TFRs of the single components. These interferences lead in most cases the TF density to be even negative in some parts of the TF plane. This last flaw can be removed by some postprocessing of the representation, which, however, reintroduces unavoidably some blur in the TF plane [22]. Furthermore, the extraction of a signal, or part of it, is much less straightforward for bilinear than for linear TFRs. To make things worse, in many practical applications, the signals under study contain several components that are highly nonstationary, with time-varying characteristics that may be important to capture as accurately as possible. For such signals, both the linear and bilinear methods show their limitations. Bilinear methods TFRs end up being corrupted by many interference terms, and even if these interferences can be mitigated, the reconstruction of the individual components would still be a hard problem to solve. Linear methods are too rigid, or provide too blurred TFRs [19].

For all these reasons in the last few years, several approaches have been proposed, like the reassignment method [2,7], the scattering transform and the time-frequency scattering [1,35], the synchrosqueezing transform and the concentration of frequency and time [3,18–20]. For a more comprehensive list and further details on these methods please refer to [53]. All these methods allow to generate a much crisper and focused TF representation of a highly nonstationary multi-components signal. However, the problem of how to properly extract chirps from a given signal remains an open problem even with these approaches. This is because they have been developed for TF analysis and they have only limited abilities in the decomposition and separation of components, especially when the noise level increases [20]. New promising results in this direction are coming from the so-called de-shape algorithm and Ramanujan de-shape method [8,32]. Furthermore, the extension of these kinds of methods to higher dimensional and multivariate signals has been only partially explored so far [34].

Two decades ago a different kind of method was introduced, the so-called Hilbert Huang Transform (HHT) [28], a local and adaptive data-driven method which has an iterative "divide et impera" approach. The idea is simple but powerful: we first iteratively divide the signal into several simple oscillatory components via the so-called Empirical Mode Decomposition (EMD) method, then each of them is analyzed separately in the TF domain via the well-known Hilbert transform, i.e. the computation of the instantaneous frequency of each component [27,30]. This approach allows us to bypass in part the Heisenberg-Gabor uncertainty principle [22], overcoming, in particular, artificial spectrum spread caused by sudden changes. EMD allows to extract each simple oscillatory component via the subtraction of the signal moving average which is computed as the average between two envelopes connecting its minima and maxima [28]. These simple oscillatory components have been named intrinsic mode functions (IMFs) by Huang and collaborators [28] and are informally defined in that work as functions fulfilling two properties: the number of extrema and the number of zero crossings must either equal or differ at most by one; the mean between an upper envelope, connecting all the local maxima, and a lower envelope, connecting all the local minima of the function, has to be zero at any point.

The decompositions produced using the EMD algorithm proved to be successful for a wide range of applications, like, for example, [16,29,40,49,50,56]. Nevertheless, the EMD algorithm contains a number of heuristic and ad hoc elements that make hard its mathematical analysis, including an a priori convergence. This is because the core of the algorithm relies heavily on interpolates of signal maxima and minima. This very approach does have also some stability problems in the presence of noise, as illustrated in [54]. Several variants of the EMD have been recently proposed to address this last problem, e.g. the Ensemble Empirical Mode Decomposition (EEMD) [54], the complementary EEMD [55], the complete EEMD [51], the partly EEMD [59], the noise assisted multivariate EMD (NA-MEMD) [52]. They all allow us to address this issue as well as reduce the so-called mode mixing problem. But they pose new challenges both to our mathematical understanding of this kind of technique and to the ability of these methods to handle chirps, since they worsen the mode-splitting problem present in the EMD algorithm [55]. Given the attention that these methods received from the worldwide scientific community (Huang's papers received far more than 30000 citations based on Scopus) many other research groups started working on this topic and proposed alternative approaches to signal decomposition. We recall the sparse TF representation [24,25], the Geometric mode decomposition [57], the Blaschke decomposition [15], the Empirical wavelet transform [23], the Variational mode decomposition [21], and similar techniques [37,43,45]. All of these methods are based on optimization with respect to an a priori chosen basis.

The only alternative method proposed so far in the literature which is based on iterations, and hence does not require any a priori assumption on the signal under analysis, is Iterative Filtering (IF) algorithm [33], its fast implementation based on FFT, named Fast Iterative Filtering (FIF) [11], and their generalizations, the Adaptive Local Iterative Filtering (ALIF) [10], and Resampled Iterative Filtering (RIF) algorithms [4,5] for the handling of signals containing strongly nonstationarities, like chirps, whistles, and multipath. These alternative iterative methods, although published only recently, have already been used effectively in a wide variety of applied fields like, for instance, in [31,36,38,39,41,42,46–48,58]. The structure of the IF, ALIF and RIF algorithms resemble the structure of the EMD method. Their key difference is in the way the signal moving average is computed, i.e., via convolution of the signal itself with an a priori chosen filter function, instead of using the average between two envelopes. This apparently simple difference opened the doors to the mathematical analysis of IF, ALIF, and RIF [4,9,11,13,26,49]. In particular, in [11], and [26], the mathematical analysis of the IF algorithm was conducted and a priori conditions for the convergence of that algorithm were identified. In [9] the analysis of the boundary effects in the IF algorithm was conducted, and a formula to estimate a priori how much error can propagate inside each component of a decomposition was presented. In [49] the authors proposed a method which allows to reduce the boundary effects in all decomposition algorithm, including IF, and studied the ability of IF in separating components produced by stochastic processes. In [13] the authors, following the analysis done for EMD [60] and Synchrosqueezing [61], analyzed the ability

of IF in separating two stationary frequencies contained in a signal. Finally, in [4], [5] and [12] the authors studied the convergence of the ALIF method and proposed the alternative, faster, and convergent RIF algorithm.

In this work, we tackle the problem of building a fast, local, and reliable TFR method based on the IMFs decomposition produced by the IF–based methods. To do so, we present some new insight in the study of the IF–based methods, and we analyze in detail the properties of the derived IMFs. Based on these results we revise the newly introduced TFR technique, named IMFogram (pronounced like "infogram"), which proves to be a generalization of the spectrogram of a signal [44]. We point out that the IMFogram method requires only the IMF decomposition to produce in a fast, local, and reliable way the TFR of a signal. Therefore this method is not limited only to IF–based IMFs decompositions. IMFogram can be used to produce a TFR based on the IMFs derived by any decomposition method, like the EMD–based techniques, or any other signal decomposition method developed so far.

The rest of the work is organized as follows. In Section 2 we review the IF method, its fast implementation based on FFT, named Fast Iterative Filtering (FIF), and their main theoretical properties. Section 3 is devoted to presenting new theoretical insight into the decompositions produced by IF–based methods. Then, leveraging these new theoretical insights, we recall the IMFogram, and study its mathematical properties in Section 4. In Section 5 we show some numerical examples of applications of the newly proposed IMFogram to both artificial and real-life signals, and the comparisons with other methods, like spectrogram, also known as Short Time Fourier Transform, synchrosqueezing, and Hilbert transform-based TFRs. This work ends with an outlook on future research directions.

2. (Fast) iterative filtering

To begin, we recall briefly the Fast Iterative Filtering (FIF) method that decomposes a discrete signal s into a collection of IMFs. To keep the discussion concise, our signal is always a finite sequence $s = (s_j)_0^{n-1}$ in $\mathbb{R}^n$. This finite sequence should be viewed as a time series over the time interval $[0, L]$, evenly sampled at the rate of $2B$. More precisely, for $j = 0, 1, \dots, n-1$, $n = 2BL$,

$$t_j = \frac{j}{2B}, \quad s_j = s(t_j). \tag{1}$$

Thus, (s_j) can be viewed as a discretization of s. With a bit of abuse of notation, s refers to both the underlining signal and the discretization of the signal. From a discrete signal $s = (s_j)$ in $\mathbb{R}^n$, we can also view the signal s as a continuous function by a linear interpolation of (s_j) over the interval $[0, L]$.

For convenience, instead of using the standard 2-norm of a vector in $a = (a_k)_{1\le k\le n} \in \mathbb{R}^n$ which corresponds to a signal over a time domain [0, L], as $\left(\sum_k |a_k|^2\right)^{1/2}$, throughout the paper, we use the normalized 2-norm:

$$\|a\|_2 = \sqrt{\frac{L}{n}} \left(\sum_j |a(t_j)|^2\right)^{1/2}$$

where the function $a : [0, L] \to \mathbb{R}$ is obtained as the linear interpolation of the sequence (a_k) over the interval $[0, L]$.

The discrete Fourier transform of (s_j), $\hat{s}_k = \hat{s}(\xi_k)$, where

$$\xi_k = \frac{k}{L}, \quad k = 0, 1, \dots, n-1 \tag{2}$$

and

$$\hat{s}(\xi_k) = \sum_{j=0}^{n-1} s_j e^{-2\pi i t_j \xi_k}. \tag{3}$$

So the sampling rate for $\hat{s}$, the discrete Fourier transform of s is $\frac{1}{L}$ over the frequency interval $[0, 2B]$.

For all the signals, and later any filters, that we will consider here, we assume that they are all pre-extended to eliminate any boundary error propagation that may occur due to the usage of Fast Fourier transformation (FFT). For a detailed discussion, please see [9,49].

A key object in the iterative filtering method is the filter. We recall the definition here for completeness.

Definition 1.

(1) A function $w : [-l, l] \to \mathbb{R}$ is a filter if it is nonnegative, even, bounded, continuous, and $\int_{\mathbb{R}} w(t)\, dt = 1$.
(2) A double convolution filter w is the self-convolution of a filter $\tilde{w}$, that is $w = \tilde{w} * \tilde{w}$.
(3) The size, or the length, of a filter w is half of its support: filter length of $w = \frac{1}{2} m\{t : w(t) > 0\}$.

The definition implies that convolutions of filters are filters. In particular, the range of the Fourier transform of a filter is in $[-1, 1]$, and the range of the Fourier transform of a double convolution filter is in $[0, 1]$ [11].

We will also identify the filter w with its discretization: $w = (w_j) = (w(t_j))$, where t_j is defined as in (1). Consider a signal $s = (s_j)$ and a double convolution filter $w = (w_j)$ in $\mathbb{R}^n$. Both sequences (s_j) and (w_j) are properly extended, as mentioned earlier so that there will be no boundary error when FFT is applied.

The moving average with respect to the filter w is defined as the convolution

$$C_w s = w * s, \quad (C_w s)_j = \sum_{k=0}^{n-1} w_{k+j} s_k. \tag{4}$$

We subtract the moving average from the signal and obtain the variation of the signal around its w-moving average,

$$\mathcal{V}_w s = s - C_w * s, \quad (\mathcal{V}_w s)_j = s_j - (C_w * s)_j. \tag{5}$$

Iterating p-times the linear operator $\mathcal{V}_w$, we obtain the linear IMF operator,

$$\mathcal{I}_{w,p} = \mathcal{V}_w^p \tag{6}$$

Observe that in the frequency domain,

$$\left(\widehat{\mathcal{V}_w s}\right)_j = (1 - \widehat{w})_j (\widehat{s})_j, \quad (\widehat{\mathcal{I}_{w,p} s})_j = (1 - (\widehat{w})_j)^p (\widehat{s})_j. \tag{7}$$

Taking the inverse FFT (iFFT), we obtain the IMF from s with filter w and p iterations:

$$\text{IMF} = \text{IMF}_{w,p} = \text{iFFT}(\widehat{\mathcal{I}_{w,p} s}). \tag{8}$$

The algorithm would run infinitely many times. To have finite time computations it is possible to use a stopping criterion. In the literature, the standard stopping criterion used [33] is the relative error in norm 2

$$\frac{\|\mathcal{V}_w^{p+1}(s) - \mathcal{V}_w^p(s)\|_2}{\|\mathcal{V}_w^p(s)\|_2} \leq \delta. \tag{9}$$

We recall the following theorem from [11], which guarantees that the difference of consecutive iterations of the variation operators converges to zero as the number of iterations increases.

Theorem 1 *([11]). Let $s = (s_j)$ be a discrete signal with a double convolution filter $w = (w_j)$. Then for all p,*

$$\left\| \mathcal{V}_w^{p+1}(s) - \mathcal{V}_w^p(s) \right\|_2 \leq \frac{1}{ep} \|s\|_2. \tag{10}$$

As we see, an IMF depends on choices of the filter w and the number of iterations p. Theorem 1 provides the theoretical justification for the stopping criterion for the inner loop of the following FIF algorithm. In practice, the number of iterations for the inner loop is much smaller than the theoretical bound.

Algorithm 1 Fast Iterative Filtering IMF = FIF(s), $\delta > 0$

```
IMF = {}
while the number of extrema of s ≥ 2 do
    compute the filter length l for s and the corresponding filter w
    ŝ = FFT(s)
    ŵ = FFT(w)
    while ‖ŝ_{m+1} − ŝ_m‖_2 > δ‖s‖_2 do
        (ŝ_{m+1})_j = (Î_{w,m} s)_j, for j = 0, ..., n − 1
        m = m + 1
    end while
    IMF = IMF ∪ {iFFT(ŝ_m)}
    s = s − iFFT(ŝ_m)
end while
IMF = IMF ∪ {s}
```

In [11] we proved the convergence of FIF

Theorem 2 *([11]). Given a signal $s \in \mathbb{R}^n$, and a filter vector w derived from a symmetric filter h convolved with itself. Fixed $\delta > 0$, then, for the minimum $N_0 \in \mathbb{N}$ such that the stopping criterion (9) is satisfied, the first IMF contained in s is given by*

$$IMF = iFFT\left((I - FFT(w))^{N_0} FFT(s)\right) \tag{11}$$

Regarding the filter, we choose a double convolution filter w_0 like the Fokker-Plank filters [10], and for the length l estimation, following [33], we compute

$$l := 2\left\lfloor \chi \frac{n}{k} \right\rfloor \tag{12}$$

where n is the length of the vector s, k is the number of its extrema, χ is a tuning parameter chosen between 1.1 and 2, and usually fixed to 1.6, and $\lfloor \cdot \rfloor$ rounds a positive number to the nearest integer closer to zero. We point out that this formula computes some sort of average highest frequency contained in s.

Another possible approach could be using the Fourier spectrum of s and the identification of its highest frequency peak. The filter length l can be chosen to be proportional to the reciprocal of this value.

The Fokker-Plank filters, as well as the approaches just described for the computation of the filter length l are pretty standard, we welcome the readers to design different filters.

The computation of the filter length l is a crucial step of the FIF technique [13]. Clearly, l is strictly positive, and, more importantly, it is based solely on the signal itself. This last property makes the method nonlinear.

In fact, if we consider two distinct signals s and z of the same length over the same time interval with the same sampling rate, then in general there is no relationship between the filter length associated with s, z, and $s+z$. Hence, if $\mathrm{IMF}_1(\bullet)$ represents the first IMF extracted by FIF from a signal, then

$$\mathrm{IMF}_1(s+z) \neq \mathrm{IMF}_1(s) + \mathrm{IMF}_1(z).$$

3. New theoretical insights in nonstationary signals decomposition

In this section we present new theoretical insights into the decompositions produced using FIF–based methods and on the time-frequency representation for nonstationary signals based on the IMFs. Using these results, we can now study a new tool to study nonstationary signals named IMFogram, which was recently introduced in [6] but was not discussed in detail.

It has been well established that the 2-norm represents the energy for a signal, either discrete or continuous. It follows from the Parseval-Plancherel identity that Fourier transform is an isometry, therefore the 2-norm of an L_2 signal is the same as the 2-norm of its Fourier transform. Here we propose a new energy norm for a signal, the L_1 Fourier Energy, when it is finite.

Definition 2 *(L_1 Fourier Energy of a signal s).* Given a signal s, its L_1 *Fourier Energy* is defined as

$$E_1(s) = ||\hat{s}||_1. \tag{13}$$

In particular, if $s = (s_j) \in \mathbb{R}^n$, then $E_1(s) = \sum_k |\hat{s}(\xi_k)|$ where ξ_k is defined as in (2).

Definition 3 *(Conservation of L_1 Fourier Energy).* Let $s \in \mathbb{R}^n$ and $s = \sum_k \phi_k$ be a decomposition of s. We say that the decomposition conserves the signal L_1 Fourier Energy if and only if

$$E_1(s) = \sum_k E_1(\phi_k) \tag{14}$$

Definition 4 *(Unwanted oscillations).* Let $s \in \mathbb{R}^n$ and $s = \sum_k \phi_k$ be a decomposition of s. The decomposition $\{\phi_k\}$ contains unwanted oscillations if there exists ξ such that

$$\sum_k \left|\hat{\phi}_k(\xi)\right| > |\hat{s}(\xi)| \tag{15}$$

Our new theoretical insight is that Algorithm 1 will not produce any unwanted oscillation and the decomposition preserves the L_1 Fourier Energy norm.

Theorem 3. *Let $s \in \mathbb{R}^n$ and $\delta > 0$. Apply Algorithm 1 with w a double convolution filter, and we have $s = \sum_1^m IMF_k + r$, where r is a trend. Then this decomposition preserves the L_1 Fourier energy and produces no unwanted oscillations.*

Proof. Following Algorithm 1, let $s^{(1)} = s$, and w_1 be the associated double convolution filter. Then

$$\mathrm{IMF}_1 = \mathcal{I}_{w_1,p_1}(s^{(1)})$$

for some positive integer p_1 determined by δ, and

$$\widehat{\mathrm{IMF}}_1(\xi) = (1 - \hat{w}_1(\xi))^{p_1}\, \widehat{s^{(1)}}(\xi).$$

Inductively, for $k = 1, 2, \ldots, m-1$, define

$$s^{(k+1)} = s^{(k)} - \mathrm{IMF}_k, \quad \widehat{\mathrm{IMF}}_{k+1}(\xi) = (1 - \widehat{w_{k+1}}(\xi))^{p_{k+1}}\, \widehat{s^{(k+1)}}(\xi),$$

where w_k is the double convolution filter associated with $s^{(k)}$ and p_k is associated with the stopping criterion δ. It follows immediately that for $k = 1, 2, \dots, m$

$$\widehat{\mathrm{IMF}}_k(\xi) = \hat{s}(\xi)(1 - \widehat{w_k}(\xi))^{p_k} \prod_{j=1}^{k-1} \left(1 - (1 - \hat{w}_j(\xi))^{p_j}\right).$$

Define $f_k(\xi) = (1 - \widehat{w_k}(\xi))^{p_k} \prod_{j=1}^{k-1} \left(1 - (1 - \hat{w}_j(\xi))^{p_j}\right)$ and $f_0(\xi) = \hat{r}(\xi)$. Observe that

$$\sum_{k=0}^{m} f_k(\xi) = 1, \quad 0 \le \sum_{k=1}^{m} f_k(\xi) \le 1, \quad \text{for all sampling points } \xi,$$

therefore, $0 \le f_0(\xi) = \hat{r}(\xi) \le 1$. It follows immediately that

$$\sum_k \left|\widehat{\mathrm{IMF}}_k(\xi)\right| = \sum_{k=1}^{m} f_k(\xi) \left|\hat{s}(\xi)\right| \le \left|\hat{s}(\xi)\right|.$$

The conservation of the L_1 Fourier Energy follows from

$$\begin{aligned}\sum_{k=0}^{m} ||\widehat{\mathrm{IMF}}_k||_1 &= \sum_{k=0}^{m} \sum_j f_k(\xi_j) \left|\hat{s}(\xi_j)\right| = \sum_j \sum_{k=0}^{m} f_k(\xi_j) \left|\hat{s}(\xi_j)\right| \\ &= \sum_j \left|\hat{s}(\xi_j)\right| = ||\hat{s}||_1 \quad \square\end{aligned}$$

An important result that follows from Theorem 3 is that, intuitively speaking, the Fourier transforms of the first IMF contains, for every fixed frequency ξ, a percentage, precisely $f_1(\xi) = (1 - \hat{w}_1(\xi))^{p_1}$, of $\hat{s}(\xi)$, i.e. the original signal Fourier transforms at frequency ξ. Subsequent IMFs contain at ξ a percentage of the leftover signal Fourier transforms in ξ. For instance the second IMF Fourier transform contains at ξ the percentage $f_2(\xi) = (1 - \hat{w}_2(\xi))^{p_2} \left(1 - (1 - \hat{w}_1(\xi))^{p_1}\right)$, which is the $(1 - \hat{w}_2(\xi))^{p_2}$ of the percentage $\left(1 - (1 - \hat{w}_1(\xi))^{p_1}\right)$ leftover in the signal after subtracting the first IMF. The very same reasoning applies to all the subsequent IMFs. This observation allows us to state in an intuitive way that, when we add together all the IMFs from the first to the m-th one, the $\sum_{k=1}^{m} \widehat{\mathrm{IMF}}_k(\xi)$ is given by the complex number $\hat{s}(\xi)$ multiplied by a real number in the interval $[0,\ 1]$. Furthermore, this number is strictly monotonically increasing and tends to 1 as $m \in \mathbb{N}$ grows.

Furthermore, this theorem justifies our definition of L_1 Fourier Energy, energy conservation, and what can be considered as an unwanted oscillation potentially produced by FIF methods. This implies also that the conservation of L_1 Fourier Energy in FIF–based methods is all we need to guarantee the meaningfulness of the decomposition. In particular, Theorem 3 allows us to conclude that, when we apply FIF to any signal, the IMFs produced do not contain any energy contribution coming from the filter w. The oscillations contained in the IMFs they are all originated from the energy contained in the signal under investigation. The filter w contributes only to the way this energy is split among the different IMFs.

It is important to point out that unwanted oscillations and mode-mixing are two distinct concepts. Unwanted oscillations represent energy injected in the IMFs by the decomposition method, whereas mode-mixing represents the presence of two or more frequencies in a single IMF [54]. Theorem 3 guarantees that FIF will not produce unwanted oscillation in the decomposition of any signal. However, based on this theorem, nothing can be concluded regarding the mode-mixing in a decomposition produced by FIF. All is known so far is that, based on numerical results, the IMFs produced by FIF are close to be mutually orthogonal, if the filter length selection is done properly and following the information contained in the data. This implies that mode-mixing is almost absent in a decomposition produced by FIF. Nevertheless, studying this problem goes beyond the scope of the present work. We leave it to future work.

3.1. Example of FIF with a bad choice for the filter

If we run FIF with a filter that is not a double convolution filter we may end up introducing unwanted oscillations in the decomposition.

In Fig. 1, left panel, we plot the signal $s(t)$ obtained as composition of the two non-stationary components

$$\begin{aligned} s_1(t) &= \cos\left(480\pi t^2 + 240\pi t\right) \\ s_2(t) &= \cos\left(\pi t^3 + 36\pi t^2 + 24\pi t + 2\pi\right), \qquad \text{where } t \in [0,\ 1]. \end{aligned} \tag{16}$$

In Fig. 1, the central panel, it is shown the FIF decomposition into two IMFs obtained using a Fokker-Planck filter [10], which has not been convolved with itself. It is already evident from this plot that the algorithm is not converging to a meaningful solution and that unwanted oscillations become present. If we look at the absolute values of the Fourier coefficients of the original signal versus the summation of the absolute values of the Fourier coefficients of two IMFs produced, Fig. 2 left column, we have the confirmation that the L_1 Fourier Energy of the signal is clearly not conserved in this case.

If, instead, we consider the same Fokker-Planck filter used in the previous passage and, before applying it in the FIF algorithm, we convolve it with itself, then, by Theorem 3, we are guaranteed a priori that the L_1 Fourier Energy of the signal will be conserved

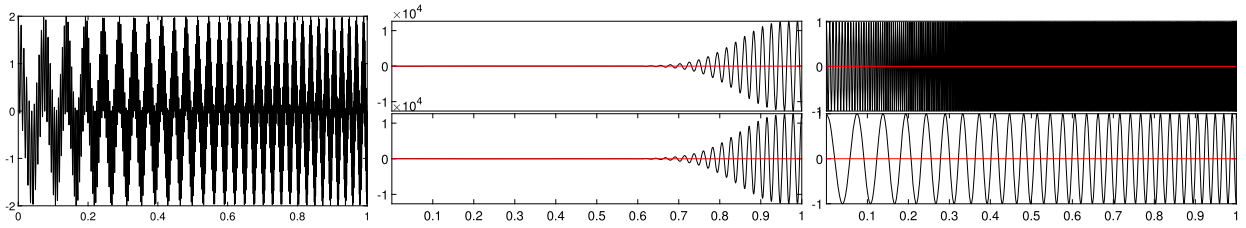

Fig. 1. First example: FIF run with a bad choice of the filter. Left panel, signal. Central panel, FIF decomposition using a Fokker-Planck filter without convolving it with itself. Right panel, FIF decomposition using a filter obtained as convolution of a Fokker-Planck filter with itself.

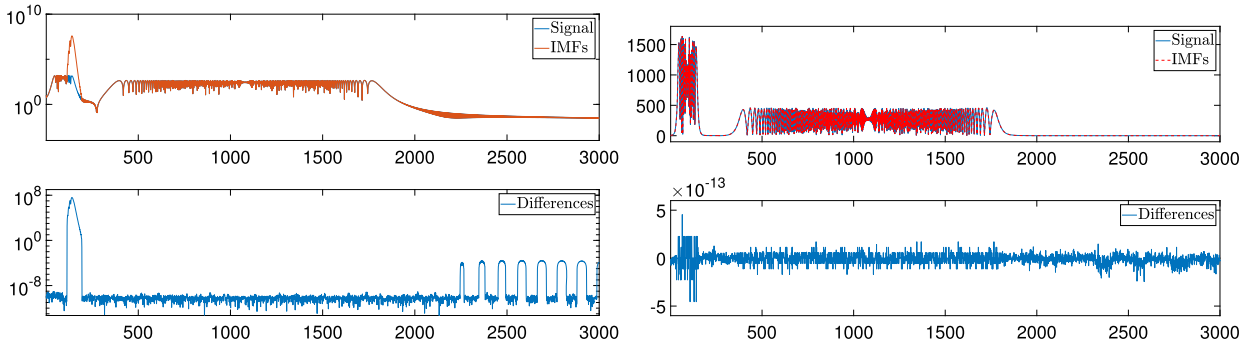

Fig. 2. First example. First row: the absolute value of the signal FFT compared with the sum of the absolute values of the IMFs FFT. Left panel, FIF with a bad choice of the filter, right panel, FIF with a double convolution filter. Second row the differences between the absolute value of the signal FFT and the sum of the absolute values of the IMFs FFT, left when the filter does not guarantee the convergence of FIF, right when the filter is chosen appropriately. (For interpretation of the colors in the figure(s), the reader is referred to the web version of this article.)

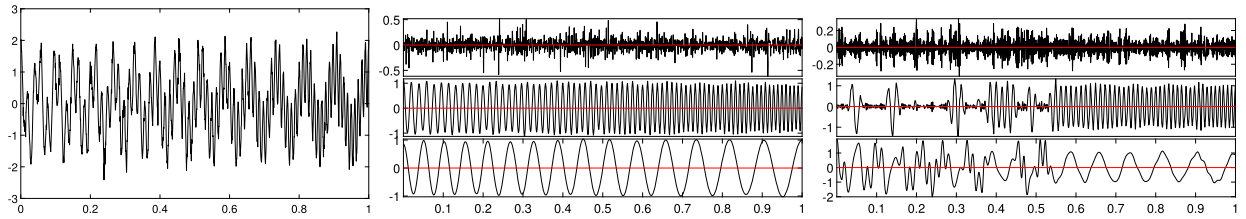

Fig. 3. Second example. Left panel, the signal. The central panel, FIF decomposition with a double convolution filter. Right panel, EMD decomposition.

and, even more importantly, no unwanted oscillation will appear. This is confirmed by looking at the numerical results plotted in Fig. 1 right panel, where the newly produced IMFs are depicted and no unwanted oscillations are visible naked eye. Furthermore, the absence of unwanted oscillations is confirmed also by looking at the absolute values of the Fourier coefficients of the original signal versus the summation of the absolute values of the Fourier coefficients of these two newly obtained IMFs, Fig. 2 right column. The differences between these two curves, which are plotted in the bottom row, second column of Fig. 2, is around machine precision.

3.2. Example of EMD decomposition

The previous definition of unwanted oscillations has been tailored on IF–based technique decompositions, but it can be tested also on other signal decompositions. For instance, the EMD algorithm is well known to be unstable in the presence of noise [54]. In this example, we compare the FIF and EMD decomposition of a nonstationary signal $s(t) = s_1(t) + s_2(t)$, where s_1 and s_2 are defined in (17), perturbed by a component $s_3(t)$, which is stationary in frequency at 200 Hz, and whose amplitude $A(t)$ is a white Gaussian noise distribution whose four statistical momenta are $\mu = 0$, $\sigma = 0.18$, skewness 0.17 and kurtosis 6.

$$\begin{aligned} s_1(t) &= \cos\left(50\pi t^2 + 100\pi t\right) \\ s_2(t) &= \cos\left(-10\pi t^2 + 40\pi t\right) \\ s_3(t) &= A(t)\cos(400\pi t), \qquad \text{where } t \in [0,\, 1]. \end{aligned} \tag{17}$$

From the rightmost panel of Fig. 3, we can see that a mode mixing problem arises when we apply EMD to decompose the signal. This is due to the local instability of the decomposition that affects the classical EMD method [54]. Many generalizations of the EMD have been proposed in the last decade to fix this issue, as we mentioned in the introduction. It is important to recall here that the IF

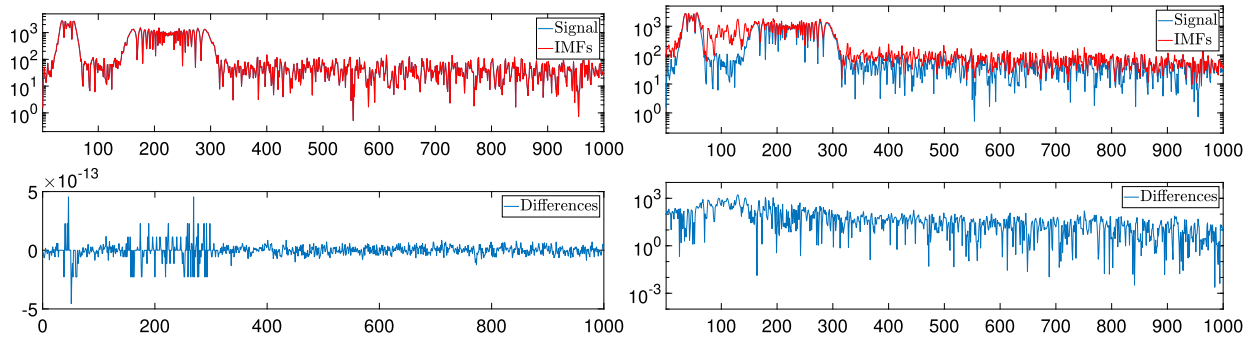

Fig. 4. Second example. The absolute value of the signal FFT compared with the sum of the absolute values of the IMFs FFT when we apply FIF or EMD decomposition, respectively left and right columns.

and FIF algorithms are not prone by construction to mode mixing. In Fig. 4 we plot the absolute values of the signal FFT as well as the sum of the absolute values of the IMFs FFT, for both the FIF and EMD decomposition, as well as their differences, bottom row. From these results, it is evident that FIF, as expected from the theory, conserves the L_1 Fourier Energy of the signal, whereas EMD decomposition does not conserve it. However, we remind that this result does not allow us to derive any further conclusion on the EMD, more than the mode mixing is reflecting, as expected, also in the frequency domain. Theorem 3, in fact, can be proved only for FIF algorithm.

4. On the time-frequency representation of the IMFs

In this section, we recall the IMFogram technique for the time-frequency representation of signals, which was first introduced in [6]. Here we will give a more in-depth analysis of the IMFogram and comparisons to other time-frequency representations.

It is by design that each IMF has a small range of frequency with a relatively large amplitude. With this in mind, we start by defining the *local amplitude*, and *local frequencies* of an IMF.

It is important to point out that classical methods based on Fourier and wavelet transforms implicitly assume that each component contained in the signal presents only interwave modulation, i.e. modulation from one period to the next one, in frequency and amplitude, and not intrawave modulation, i.e. modulation inside each period. This is a consequence of the choice of sinusoidal bases in the Fourier transform, or the choice of a fixed predefined mother wavelet that is used to build all other wavelets in the wavelet transform. From now on, following the same kind of reasoning, we make the assumption that each component contained in the signal presents only interwave modulation in frequency and amplitude, and not intrawave modulation. This is a strong assumption, however, it allows us to build a time-frequency representation based on IMFs which, as we will prove in the following, converges to the spectrogram representation for a certain class of signals. Developing a time-frequency representation based on IMFs that can capture the intrawave modulations contained in them remains an open problem that deserves to be studied in future work.

Definition 5 *(Instantaneous amplitude and Instantaneous frequency function for an IMF).* Fix an $\mathrm{IMF} = (\mathrm{IMF}(t_j))_0^{n-1}$.

(1) Let g be the linear interpolation of the local maximum of $|\mathrm{IMF}|$. The *instantaneous amplitude function* for this IMF, is defined as $iA^{\mathrm{IMF}} : [t_0, t_{n-1}] \to \mathbb{R}$, the linear interpolation of $(t_j, iA^{\mathrm{IMF}}(t_j))$, where $iA^{\mathrm{IMF}}(t_j) = \max\{g(t_j), |\mathrm{IMF}(t_j)|\}$.
(2) Let f be the linear interpolation of $\mathrm{IMF}(t_j)$ over the interval $[t_0, t_{n-1}]$, and denote the zero crossings of f by $\{z_1 < z_2 < \cdots < z_p\}$. For $j = 1, 2, \ldots, p$, define $y_j = \frac{1}{z_{j+1} - z_j}$, $z_0 = t_0$, and $z_{p+1} = t_{n-1}$, $y_0 = y_1$, $y_{p+1} = y_p$. The *instantaneous frequency function*, $iF^{\mathrm{IMF}} : [t_0, t_{n-1}] \to \mathbb{R}$ is the linear interpolation of $\{(z_j, 2y_j)\}_{j=0}^{p+1}$.

The instantaneous amplitude and instantaneous frequency of IMF at t_j is $iA^{\mathrm{IMF}}(t_j)$ and $iF^{\mathrm{IMF}}(t_j)$ respectively. By slightly abuse of notation, if we identify the discrete sequence IMF with its linear interpolation function, the instantaneous amplitude and instantaneous frequency of IMF at $t \in [t_0, t_{n-1}]$ is simply $iA^{\mathrm{IMF}}(t)$ and $iF^{\mathrm{IMF}}(t)$ respectively.

We observe that the choice of the envelope in the computation of the instantaneous amplitude and frequency is not stringent for the IMFogram method, since all that is needed in this context is the computation of a local amplitude and frequency which is produced as an average of the instantaneous values. In the following, to construct the envelopes, we use linear interpolation for simplicity.

As one knows, the concept of instantaneous frequency and amplitude are not universally accepted. The purpose of the last definition is to fix the terminology and not to start a philosophical discussion. Our goal is to use the instantaneous frequency and amplitude to define a version of local frequency and amplitude.

Fix the size of the time window to be the positive integer J. Consider the $n \times n$ matrix (for simplicity, we assume that n is a multiple of J) T, the averaging matrix, defined as

$$T_{i,k} = \begin{cases} 1/J, & 1+(p-1)J \le i,k \le pJ, \text{ for } p = 1,2,\dots,n/J \\ 0, & otherwise, \end{cases}$$

where $T_{i,k}$ is the (i,k) - entry of T. The operator norm for T is $\|T\| = 1$, with respect to the normalized 2-norm.

Similarly for the 2-norm of a localized function. Let $s = (s_j)$ be a vector in $\mathbb{R}^n$ and t_j is defined as in (1) if $[a,b] \subset [0,L]$ in the time domain, with $a = t_i$ and $b = t_{i+k}$, then the local 2-norm of s over $[a,b]$ is

$$\|s|_{[a,b]}\|_2 = \frac{L}{n}\left(\sum_{0\le j\le k} |s(t_{i+j})|^2\right)^{1/2} \tag{18}$$

Next, we define the local amplitude and local frequency of an IMF. In practice, we observe that for any interval $[a,b]$ that is comparable to the filter length, say the length of $[a,b]$ is 2 to 5 times the length of the filter length, then $\|\mathrm{IMF}|_{[a,b]}\|_2$ and $\|iA^{\mathrm{IMF}}|_{[a,b]}\|_2$ are comparable. This is the base for the following definition of *l*ocal amplitude.

Definition 6 *(Local amplitude and Local frequency of an IMF).* Given an $\mathrm{IMF} \in \mathbb{R}^n$ and let $iA^{\mathrm{IMF}} \in \mathbb{R}^n$ and $iF^{\mathrm{IMF}} \in \mathbb{R}^n$ be the corresponding instantaneous amplitude and frequency, respectively. The average of each of them over a segment of length J is the local amplitude $\mathrm{LA}^{\mathrm{IMF}}$ and local frequency $\mathrm{LF}^{\mathrm{IMF}}$, respectively. That is

$$\mathrm{LA}^{\mathrm{IMF}} = T(iA^{\mathrm{IMF}}), \quad \mathrm{LF}^{\mathrm{IMF}} = T(iF^{\mathrm{IMF}})$$

As we have observed above, $\|T\| = 1$, thus, we have

$$\|\mathrm{LA}^{\mathrm{IMF}}\|_2 \le \|iA^{\mathrm{IMF}}\|_2.$$

Leveraging on the previous results we can introduce the TFR method named *IMFogram*, whose pseudocode for the discrete setting is detailed in Algorithm 2.

Algorithm 2 IMFogram A = IMFogram(IMFs)

M number of IMFs
N signal length
R number of overlapping time windows $I_j = [a_j,\ b_j]$
for $k = 1$ **to** M **do**
  Compute the local amplitudes $\mathrm{LA}^{(k)}_{I_j}$
  Compute the local frequencies $\mathrm{LF}^{(k)}_{I_j}$
  for $j = 1$ **to** R **do**

$$A(\mathrm{LF}^{(k)}_{I_j}, j) = A(\mathrm{LF}^{(k)}_{I_j}, j) + \mathrm{LA}^{(k)}_{I_j} \tag{19}$$

  end for
end for
return A

The proposed TFR method requires as input the IMF decomposition of a given signal. In this work, based on the theoretical results proved so far in the literature [11], we opt to use the IMFs produced by the FIF method. However, we point out, that any other alternative decomposition techniques proposed in the literature which produce IMFs can be used. As output, the IMFogram produces a matrix A which contains the local amplitudes of the various IMFs distributed by rows and columns depending on the corresponding local frequency and time window, respectively.

Regarding the choice of the time window, the IMFogram differs from the spectrogram, or similar TFR methods, since it does not require a clever choice of the time window length. The sliding time window is basically required in the IMFogram to reduce the number of columns of the output matrix A. The user, in fact, can choose as the length of the sliding time window a value that goes from one sample point to the length of the signal itself.

Another important result concerning the FIF method is the following theorem proved in [13]

Theorem 4. *Given the signal $s \in \mathbb{R}^p$ defined as $s(x_k,a,f) = \cos(2\pi x_k) + a\cos(2\pi f x_k + \phi), k \in [1,\dots\ p]$, sampled at $Fs = \frac{1}{T} \gg 1$ samples/sec such that $p = n\frac{1}{T}$, where $f \in (\frac{1}{n}, 1)$, assuming w is a double convolution filter, whose filter length measures $2L+1$, such that the smallest positive zero in the DFT of w corresponds to frequency 1.*

Then FIF algorithm without stopping criterion can always resolve s into the two components $\cos(2\pi x_k)$ and $a\cos(2\pi f x_k + \phi)$, as far as $f \le 1 - \frac{1}{n}$.

As an immediate corollary of this theorem, we have that

Corollary 1. *Given a multicomponent signal* $s = \sum_{j=1}^{N} a_j \cos(2\pi f_j x_k + \phi_j)$, $k \in [1, \dots\ p]$, *sampled at* $Fs = \frac{1}{T} \gg 1$ *samples/sec such that* $p = n\frac{1}{T}$, *where* $f_j \ll \frac{1}{2T}$, $\forall\, j = 1, \dots, N$, $\frac{f_{j+1}}{f_j} \in (\frac{1}{n}, 1 - \frac{1}{n}), \forall\, j = 1, \dots, N-1$, *and* $\frac{a_j}{a_h} = O(1), \forall j, h = 1, \dots, N$. *Assuming that to extract each IMF component we are using a double convolution filter* w_j, *whose filter length measures* $2L_j + 1$, *such that the smallest positive zero in the DFT of* w_j *corresponds to the frequency* f_j.

Then FIF algorithm without stopping criterion can always resolve s *into* N *IMF components* $a_j \cos(2\pi f_j x_k + \phi_j)$, $j = 1, \dots, N$.

The proof follows directly from the previous theorem and the observation that FIF, as any EMD–like method, produces all the IMFs by subsequent subtraction from the signal, starting from the highest frequency component to the lowest one.

Based on these results, we are now ready to prove the following

Theorem 5. *Given a discrete nonstationary signal* $s \in \mathbb{R}^p$, *sampled at* $Fs = \frac{1}{T} \gg 1$ *samples/sec such that* $p = n\frac{1}{T}$, *and which we assume to be stationary on* K *non-overlapping time windows* I_i, $i = 1, \dots, K$, *of length* $L = \frac{p}{K}$, *assuming that in each time interval* I_i *the signal is given by* $s(I_i) = \sum_{j=1}^{N_i} a_j^{(i)} \cos(2\pi f_j^{(i)} x_k + \phi_j^{(i)})$, $x_k \in I_i$, $\frac{f_{j+1}^{(i)}}{f_j^{(i)}} \in \left(\frac{1}{n}, 1 - \frac{1}{n}\right)$, *for every* $j = 1, \dots, N_i - 1$, *and* $\frac{a_j^{(i)}}{a_h^{(i)}} = O(1), \forall\, j, h = 1, \dots, N_i$, *if we let the FIF stopping criterion* δ *to go to zero, then the Hadamard power two of the IMFogram matrix* A *converges to the spectrogram matrix obtained as the entry-wise squared absolute value of the DFT of the matrix* $S \in \mathbb{R}^{L \times K}$, *which contains in each column the non-overlapping time windows* I_i, $i = 1, \dots, K$, *of length* L *of the signal.*

Proof. We start considering a single time window I_i. From Corollary 1 follows that FIF, when $\delta \to 0$, ends up separating the signal $s(I_i) = \sum_{j=1}^{N_i} a_j^{(i)} \cos(2\pi f_j^{(i)} x_k + \phi_j^{(i)})$ into the N_i IMFs $a_j^{(i)} \cos(2\pi f_j^{(i)} x_k + \phi_j^{(i)})$, $j = 1, \dots, N_i$. Furthermore, based on Definition 6, the local frequency will be $\mathrm{LF}_{I_i}^{(j)} = f_j^{(i)}$ and the local amplitude will be $\mathrm{LA}_{I_i}^{(j)} = a_j^{(i)}$. Therefore, from Algorithm 2 it follows that the matrix A will contain in the i-th column and at rows corresponding to frequencies $f_j^{(i)}$ the values $a_j^{(i)}$, $j = 1, \dots, N_i$. These amplitudes match the Fourier coefficients computed via Discrete Fourier Transform in the interval I_i at frequencies $f_j^{(i)}$'s. The same result applies for all intervals I_i, $i = 1, \dots, K$. Hence, the entry-wise power two of the matrix A, i.e. the Hadamard power two of the matrix A, converges to the spectrogram of the signals s computed on K non-overlapping time windows of length L as the FIF stopping criterion δ goes to 0. □

We point out that if we consider a time window in the IMFogram that matches the length of the signal, the proposed TFR method boils down to a periodogram of the signal.

It is important to highlight here that the TFR produced by IMFogram and spectrogram/periodogram are different in nature when the signal under study is not stationary inside time windows. In this more general scenario, their difference is due to the fact that the IMFogram uses information coming from the time domain, local periods, and local amplitudes, to produce the TFR. Whereas, the spectrogram and periodogram, depending if we window or not the signal, use information coming from the frequency domain to produce the TFR. This explains why IMFogram can be more local in its TFR. The IMFogram does not need to extract frequency information from the Fourier transform of signal windows. Furthermore, this windowing is the main cause of artifacts in the spectrogram. In fact, if on the one hand, the Heisenberg uncertainty principle cannot be eliminated, on the other hand, the IMFogram allows removal of the uncertainties coming from the necessity, in the spectrogram and equivalent methods, of windowing the signal on sufficiently long time windows to reduce the local boundary effects induced by the Fourier Transform.

Another important observation regards how, in acoustics, a vibrato (frequency modulation with stationary amplitude) of a musical instrument can be perfectly reproduced by an expert musician as an amplitude modulation of a stationary frequency signal, what it is called an amplitude modulated monochromatic signal. With this knowledge, we observe that, while the TFR methods based on Fourier Transforms, like the well-known periodogram and spectrogram, make use of stationary amplitude components to represent a nonstationary signal, the IMFogram, based on FIF–like decompositions, tends to represent a quasi–stationary frequency signal with modulated amplitude. From this perspective, the IMFogram is a new and complementary way of looking at a signal with respect to standard TFR methods.

5. Numerical examples

In this section, we present a few synthetic and real-life examples of the application of the IMFogram algorithm as well as its comparisons with other classical methods. In particular, we compare IMFogram with spectrogram (STFT), continuous wavelet transform (CWT), synchrosqueezing transform (SST), and Hilbert Huang transform (HHT).

The following tests have been conducted using MATLAB® R2021a installed on a 64–bit Windows 10 Pro computer equipped with an Intel® Core® i7-8550U at 1.80GHz CPU and 16GB RAM. All tested examples and algorithms are freely available online.[1] For all the following examples, to produce a decomposition with FIF we used the Fokker-Plank filter developed in [10], and we use as a stopping criterion the formula (9) with a value $\delta = 0.001$.

[1] www.cicone.com.

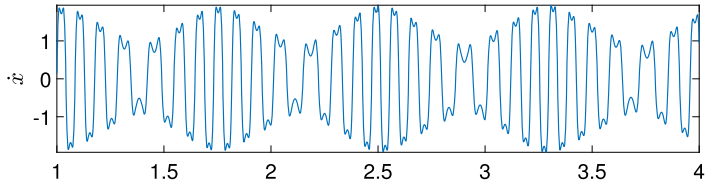

Fig. 5. Duffing equation example: the $\dot{x}$ solution of (21).

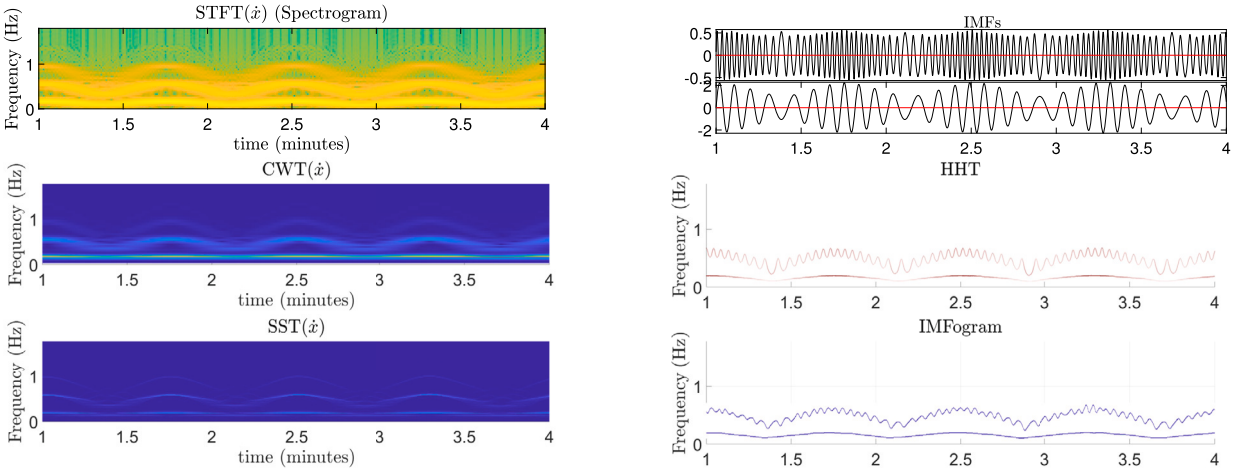

Fig. 6. Duffing equation example: In the first column, we plot the STFT, CWT, and SST representation of the $\dot{x}$ solution of (21), respectively first, second, and third row of the first column. Second column, we show the Fast Iterative Filtering decomposition into IMFs of $\dot{x}$, the HHT, and the IMFogram of these IMFs, respectively first, second, and third row of the second column.

5.1. Synthetic example – undamped Duffing equation

As a first example, we consider the synthetic signal generated as the solution of the undamped Duffing equation

$$\ddot{x} + \alpha x + \beta x^3 = \gamma \cos(\omega t), \tag{20}$$

where α represents the linear stiffness, β the nonlinearity in the restoring force, γ the amplitude, ω the angular frequency of the forcing term. We can also rewrite (20) to read

$$\ddot{x} + \left(\alpha + \beta x^2\right) x = \gamma \cos(\omega t), \tag{21}$$

where $(\alpha + \beta x^2)$ is the nonlinear stiffness coefficient $k(x)$.

In Fig. 5 we plot the $\dot{x}$ solution of (21) when $\alpha = -1$, $\beta = 1$, $\gamma = 0.1$, and $\omega = 1$. The signal under investigation apparently contains two superimposed oscillatory components. In Fig. 6 we report the STFT, CWT, and SST representation of $\dot{x}$. From all these TFR plots, it appears that three nonstationary frequency components are contained in the signal. However, if we decompose, instead, the signal into IMFs, we discover that there are actually only two components contained in this signal, Fig. 6 second column. If we apply the HHT and the IMFogram, we obtain the TFRs plotted in the second column of Fig. 6. Using these two plots it is possible to solve the riddle. The high-frequency component is modulated in frequency at a high pace. In fact, the frequency of that component varies from period to period. It is evident from this example that it is not possible for methods based on wavelet or sinusoidal bases to capture properly such behavior. By comparing the HHT, right column second row in Fig. 6, with the IMFogram, right column bottom row in Fig. 6, we can see that both methods are able to produce a good TFR of the signal. However, it is important to mention that the HHT requires in this particular example an ad hoc tuning of the IMFs amplitudes to produce the result plotted in Fig. 6. Otherwise, the first highest frequency component instantaneous frequency curve would not be visible in the plot. Whereas, the IMFogram did not require any special tuning to produce the result shown in Fig. 6.

Furthermore, we underline that it is not sufficient to decompose the signal into IMFs to obtain a higher accuracy in its TFR. In Fig. 7 we show that, even if we first split the signal into two IMFs and then apply the SST to them, the TFR obtained contains the same artificial harmonics seen when we studied the whole signal, Fig. 6.

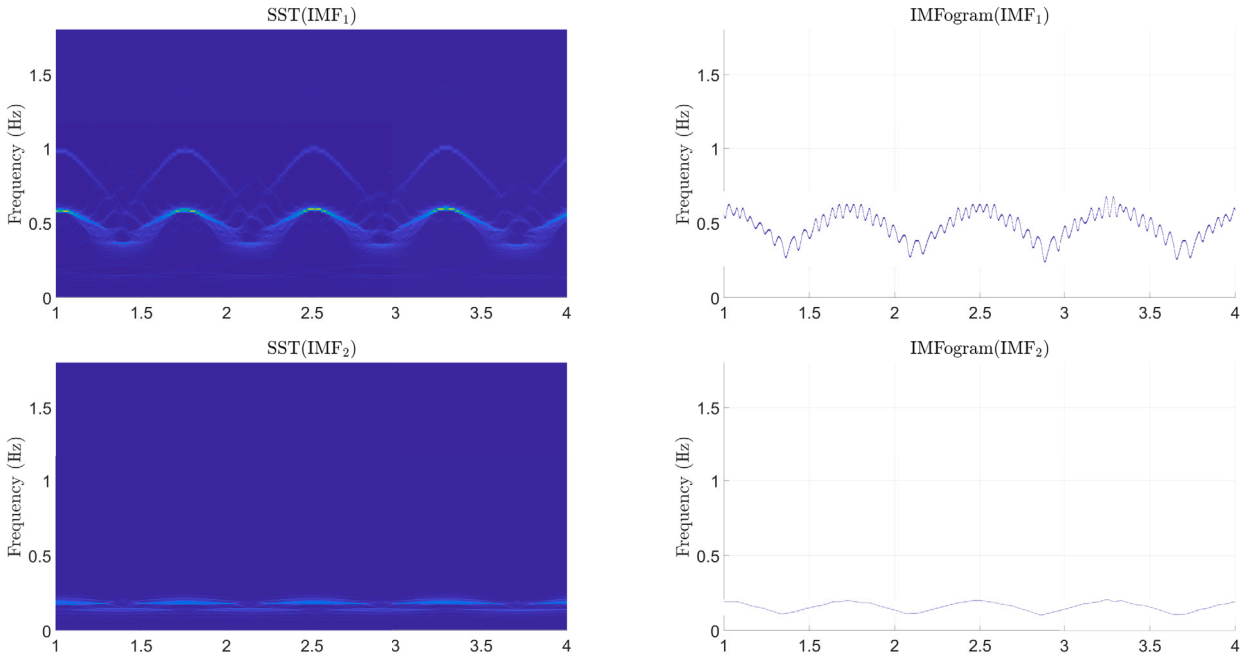

Fig. 7. Duffing equation example: Time-Frequency representations of each IMF using SST (left column) and IMFogram (right column). First row IMF_1, second row IMF_2.

5.2. Real life example – violin vibrato

In this real-life example, we consider the recording of a violin when a G open string is played with vibrato.[2] The signal is plotted in Fig. 8, together with its STFT, CWT and SST representations. Furthermore, we report a few IMFs from the signal decomposition produced using the FIF algorithm. In the bottom row of this figure, we report both HHT and IMFogram TFRs. The HHT is clearly having problems properly capturing the instantaneous frequencies contained in this signal. The IMFogram, instead, proves able to provide a crisp and clear representation of the time-frequency behavior of this signal which is, at first view, comparable with the quality of the signal SST representation. However, with a more accurate analysis, we can observe how the IMFogram contains many fine details that are completely missing in the SST representation. For instance, the oscillatory component around 800 Hz appears almost stationary in the SST representation, whereas in the IMFogram plot, it has an instantaneous frequency that is clearly oscillating.

5.3. Real life example – Earth's ionospheric electron density

In this last example, we consider the electron density (Ne), expressed in cm^{-3}, as measured in the topside ionosphere by the Langmuir Probes onboard one of the three spacecrafts constituting the Swarm[3] constellation of the European Space Agency [62]. As an example, we consider the Ne samples measured at a 2 Hz rate by the Swarm Alpha satellite between 15:39 UT and 15:58 UT on 8 September 2017, covering the auroral and polar ionospheric sectors (magnetic latitudes below 55° S) of the southern hemisphere, Fig. 9 first row. The selected date is characterized by severe geomagnetic storm conditions triggered by Coronal Mass Ejections [64] that struck the Earth's ionosphere, and caused the formation of ionospheric irregularities with largely varying spatial scales in the high-latitude ionosphere [63]. Swarm Alpha satellite flies in a quasi–polar orbit and, in the selected period, its speed was about 7.5 km/s and its altitude ranges between 440 km and 470 km.

From Fig. 9 we can see that the STFT cannot achieve a high time-frequency localization accuracy, whereas the CWT can allow for a more accurate TFR.

In Fig. 10, first row, we show how the SST can improve, as expected theoretically [18,19], the time and frequency localization obtained using the classical CWT. If we decompose the signal first into IMFs, then we can produce the HHT and IMFogram TFRs, which are plotted in the middle and bottom row of Fig. 10. From these last two panels, we can see that the HHT has problems, at least in this example, capturing in an accurate way the energy and frequency of the IMFs, whereas the IMFogram proves to be really accurate, producing a plot that is even crisper and more focused than the SST.

[2] https://en.wikipedia.org/wiki/File:Violin_vibrato_on_open_string_notes_and_on_fingered_notes.ogg.

[3] The Swarm dataset is the "2 Hz Langmuir Probe Extended Dataset" and it is provided by the European Space Agency (ESA) at swarm-diss.eo.esa.int and at http://vires.services.

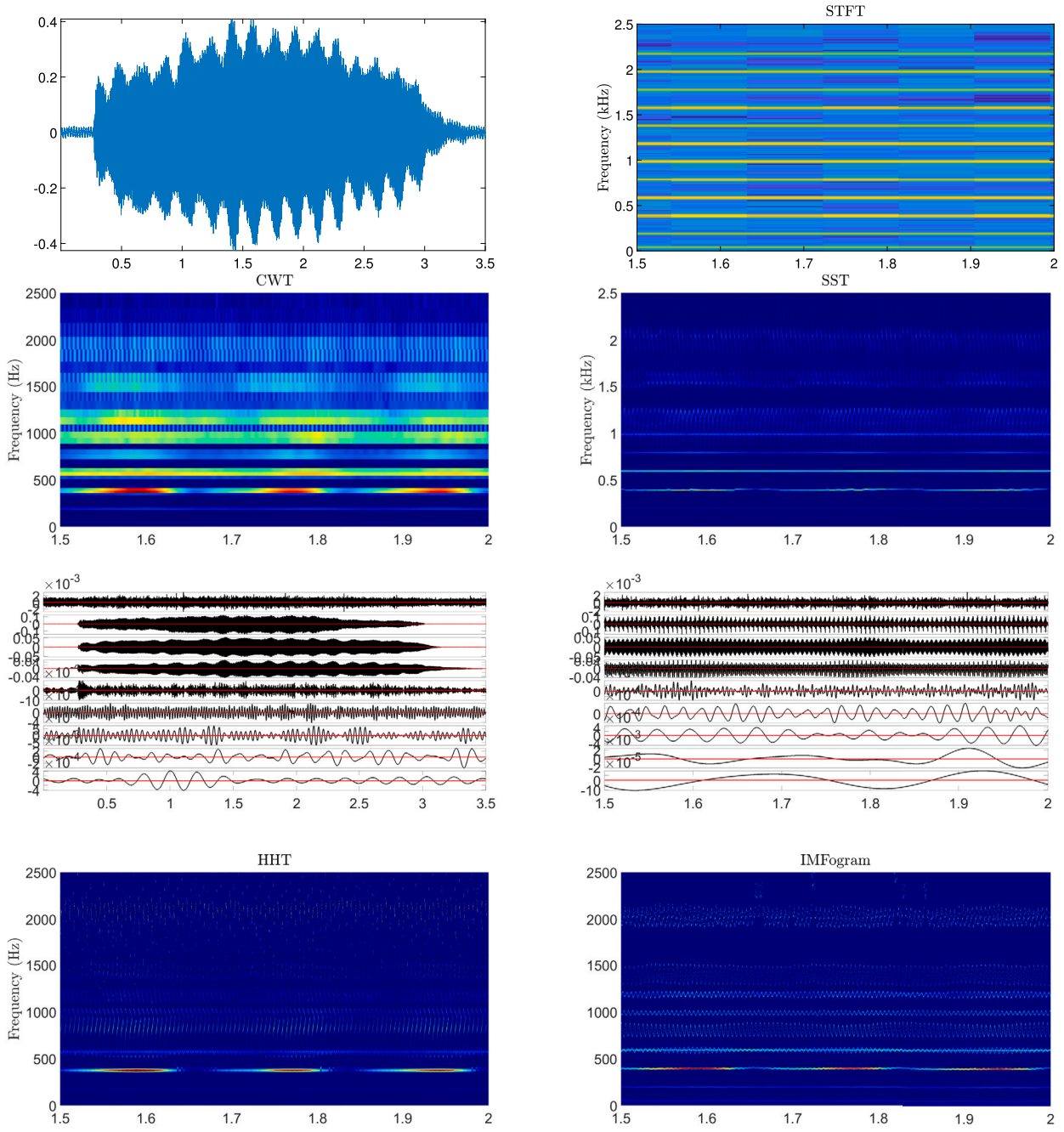

Fig. 8. Violin vibrato example: in the first row we plot the signal (left) and its STFT (right). In the second row, we show the CWT (left) and SST representation (right). In the third row the signal IMF decomposition produced by the FIF algorithm, left, and its zoomed-in version in the time interval [1.5, 2] seconds, right. Bottom row, the HHT of the IMFs (left), and the IMFogram (right).

6. Conclusions

In many real-life applications, the focus is on the time-frequency analysis of nonstationary signals. Many classical methods, like short-time Fourier transform, and continuous wavelet, and modern techniques, like reassignment, synchrosqueezing, and alternative algorithms, prove to have limitations in producing crisp and focused time-frequency representations of signals. By leveraging on the groundbreaking idea of first decomposing a given signal into simple oscillatory components, also known as intrinsic mode functions (IMFs), and then applying to each of them a time-frequency analysis, in this work we present the innovative IMFogram time-frequency representation method, and its numerical analysis. In particular, after reviewing known theoretical properties of the so-called Fast Iterative Filtering (FIF) method for the decomposition of a signal into IMFs, we propose new theoretical results regarding FIF and

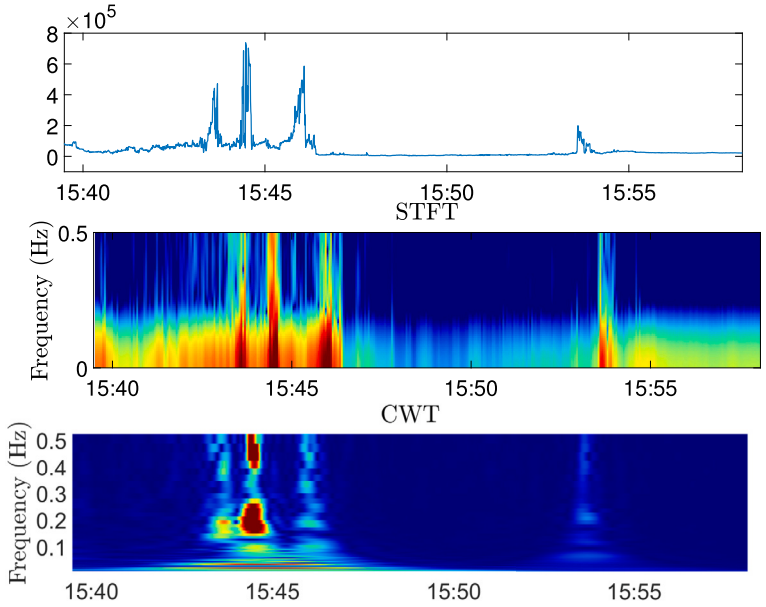

Fig. 9. Ionospheric electron density example: in the first row we plot the electron density (Ne) signal sampled by the ESA Swarm Alpha satellite between 15:39 UT and 15:58 UT on 8 September 2017. In the second and third row, we report its STFT and CWT, respectively.

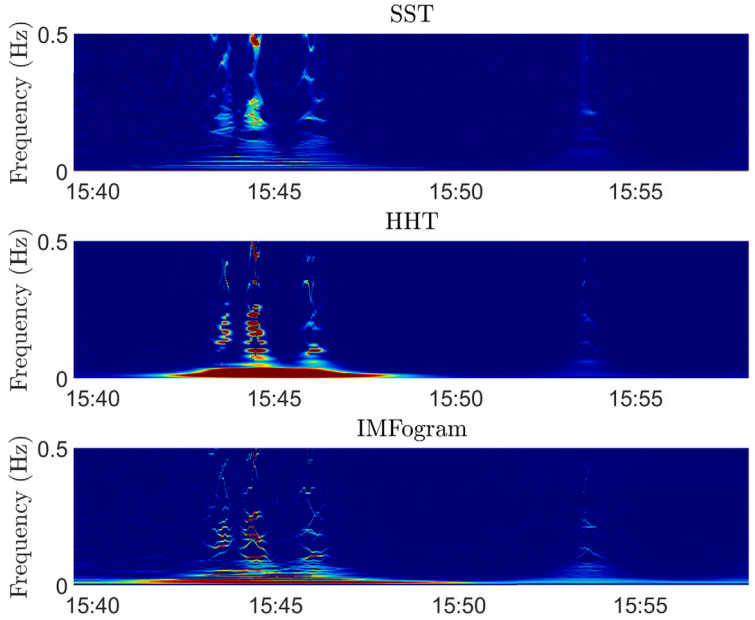

Fig. 10. Ionospheric electron density example: in the first row we show the SST representation of the sampled electron density. In the second and third row, we present its HHT and IMFogram TFRs, respectively.

IMFogram. For FIF, we prove that the algorithm can preserve the "L_1 Fourier Energy" of the signal, which allows us to prove that FIF decomposition cannot contain "unwanted oscillations", meaning that all IMFs produced by FIF are meaningful. Furthermore, for the IMFogram algorithm, we prove that, under some hypothesis on the signal, the IMFogram time-frequency representation does converge to the corresponding spectrogram as the stopping criterion δ used in FIF to produce the IMFs is sent to 0. We conclude this work with a few synthetic and real-life numerical examples showing the performance of the proposed technique.

Even though many new insights on the decomposition into IMFs and their time-frequency representation are presented in this work, many problems still remain unsolved. First of all, iterative decomposition methods, like FIF–based and EMD–based techniques, and all other methods based on optimization, like sparse time-frequency representation, empirical wavelet transform, and variational mode decomposition, just to name a few, cannot guarantee a uniqueness in the decomposition. How this can impact the associated time-frequency representation is yet to be studied.

In this work, we propose a new definition of "unwanted oscillations" produced by a decomposition method. This definition is, to the best of our knowledge, the first of its kind. We assume that other definitions of what an unwanted oscillation is can be proposed in the context of signal decomposition and we plan to work in this direction in the future.

The IMFogram convergence to the spectrogram has been proved in this work for a nonstationary signal that is piece-wise stationary. This result can be extended to more general nonstationary signals. We plan to study this problem in a separate work.

Another interesting problem regards IMFogram time-frequency representation robustness to parameters tuning in the IMFogram itself, as well as in the FIF decomposition method. This is an open research direction. We plan to tackle it in a future work.

It is also important to point out that the main step of the IMFogram algorithm, i.e. (19), is meaningful because the IMFs produced by IF and FIF methods are, based on numerical evidence we collected so far, in general quasi–orthogonal. However, this fact has not been proven rigorously yet. We plan to study this aspect in another work.

Finally, we point out that the proposed IMFogram time-frequency representation algorithm is based on the strong assumption that during each period of oscillation, the IMFs have a constant instantaneous frequency. This is true for signals having interwave modulation of their frequencies. The very same assumption is made, implicitly, in all classical methods based on Fourier and wavelet transforms. However, many real-life signals show what is called an intrawave modulation of their instantaneous frequencies. There is a need to develop a more general time-frequency representation able to handle also such intrawave modulations. This will be the subject of future work.

Data availability

Data will be made available on request.

Acknowledgments

AC is a member of the INdAM Research group GNCS and is supported in part by the Italian Ministry of the University and Research under a PRIN PNRR 2022 grant number E53D23018040001 ERC field PE1 project P2022XME5P titled "Circular Economy from the Mathematics for Signal Processing prospective". WSL is partially supported by a Simon Foundation Collaboration Grant for Mathematicians. HZ is supported in part by NSF under grants DMS-2307465, and ONR N00014-21-1-2891.

References

[1] J. Andén, V. Lostanlen, S. Mallat, Joint time–frequency scattering, IEEE Trans. Signal Process. 67 (14) (2019) 3704–3718.
[2] F. Auger, P. Flandrin, Improving the readability of time-frequency and time-scale representations by the reassignment method, IEEE Trans. Signal Process. 43 (5) (1995) 1068–1089.
[3] F. Auger, P. Flandrin, Y.-T. Lin, S. McLaughlin, S. Meignen, T. Oberlin, H.-T. Wu, Time-frequency reassignment and synchrosqueezing: an overview, IEEE Signal Process. Mag. 30 (6) (2013) 32–41.
[4] G. Barbarino, A. Cicone, Conjectures on spectral properties of ALIF algorithm, Linear Algebra Appl. 647 (2022) 127–152.
[5] G. Barbarino, A. Cicone, Stabilization and variations to the ALIF algorithm: the fast resampled iterative filtering method, Numer. Math. (2024), https://doi.org/10.1007/s00211-024-01394-y, online, arXiv:2111.02764.
[6] Ph. Barbe, A. Cicone, W.S. Li, H. Zhou, Time–frequency representation of nonstationary signals: the IMFogram, Pure Appl. Funct. Anal. 7 (1) (2022) 27–39.
[7] E. Chassande-Mottin, F. Auger, P. Flandrin, Time-frequency/time-scale reassignment, in: Wavelets and Signal Processing, Springer, 2003, pp. 233–267.
[8] Z. Chen, H.-T. Wu, When Ramanujan meets time-frequency analysis in complicated time series analysis, preprint, arXiv:2004.00076, 2020.
[9] A. Cicone, P. Dell'Acqua, Study of boundary conditions in the iterative filtering method for the decomposition of nonstationary signals, J. Comput. Appl. Math. 373 (2020) 112248.
[10] A. Cicone, J. Liu, H. Zhou, Adaptive local iterative filtering for signal decomposition and instantaneous frequency analysis, Appl. Comput. Harmon. Anal. 41 (2) (2016) 384–411.
[11] A. Cicone, H. Zhou, Numerical analysis for iterative filtering with new efficient implementations based on FFT, Numer. Math. 147 (1) (2021) 1–28.
[12] A. Cicone, C. Garoni, S. Serra-Capizzano, Spectral and convergence analysis of the discrete ALIF method, Linear Algebra Appl. 580 (2019) 62–95.
[13] A. Cicone, S. Serra-Capizzano, H. Zhou, One or two frequencies? The iterative filtering answers, Appl. Math. Comput. 462 (2023) 128322.
[14] L. Cohen, Time-Frequency Analysis, vol. 778, Prentice Hall, 1995.
[15] R.R. Coifman, S. Steinerberger, H.-t. Wu, Carrier frequencies, holomorphy, and unwinding, SIAM J. Math. Anal. 49 (6) (2017) 4838–4864.
[16] D.A. Cummings, R.A. Irizarry, N.E. Huang, T.P. Endy, A. Nisalak, K. Ungchusak, D.S. Burke, Travelling waves in the occurrence of Dengue haemorrhagic fever in Thailand, Nature 427 (6972) (2004) 344–347.
[17] I. Daubechies, Ten Lectures on Wavelets, vol. 61, Siam, 1992.
[18] I. Daubechies, A nonlinear squeezing of the continuous wavelet transform based on auditory nerve models, Wavelets Med. Biol. (1996) 527–546.
[19] I. Daubechies, J. Lu, H.-T. Wu, Synchrosqueezed wavelet transforms: an empirical mode decomposition-like tool, Appl. Comput. Harmon. Anal. 30 (2) (2011) 243–261.
[20] I. Daubechies, Y. Wang, H.-t. Wu, Conceft: concentration of frequency and time via a multitapered synchrosqueezed transform, Philos. Trans. R. Soc. A, Math. Phys. Eng. Sci. 374 (2065) (2016) 20150193.
[21] K. Dragomiretskiy, D. Zosso, Variational mode decomposition, IEEE Trans. Signal Process. 62 (3) (2013) 531–544.
[22] P. Flandrin, Time-Frequency/Time-Scale Analysis, Academic Press, 1998.
[23] J. Gilles, Empirical wavelet transform, IEEE Trans. Signal Process. 61 (16) (2013) 3999–4010.
[24] T.Y. Hou, Z. Shi, Adaptive data analysis via sparse time-frequency representation, Adv. Adapt. Data Anal. 3 (01n02) (2011) 1–28.
[25] T.Y. Hou, M.P. Yan, Z. Wu, A variant of the emd method for multi-scale data, Adv. Adapt. Data Anal. 1 (04) (2009) 483–516.
[26] C. Huang, L. Yang, Y. Wang, Convergence of a convolution-filtering-based algorithm for empirical mode decomposition, Adv. Adapt. Data Anal. 1 (04) (2009) 561–571.
[27] N.E. Huang, Introduction to the Hilbert–Huang transform and its related mathematical problems, in: Hilbert–Huang Transform and Its Applications, 2014, pp. 1–26.

[28] N.E. Huang, Z. Shen, S.R. Long, M.C. Wu, H.H. Shih, Q. Zheng, N.-C. Yen, C.C. Tung, H.H. Liu, The empirical mode decomposition and the Hilbert spectrum for nonlinear and non-stationary time series analysis, Proc. R. Soc. Lond., Ser. A, Math. Phys. Eng. Sci. 454 (1971) 903–995, 1998.
[29] N.E. Huang, Z. Wu, A review on Hilbert-Huang transform: method and its applications to geophysical studies, Rev. Geophys. 46 (2) (2008).
[30] N.E. Huang, Z. Wu, S.R. Long, K.C. Arnold, X. Chen, K. Blank, On instantaneous frequency, Adv. Adapt. Data Anal. 1 (02) (2009) 177–229.
[31] Y. Li, X. Wang, Z. Liu, X. Liang, S. Si, The entropy algorithm and its variants in the fault diagnosis of rotating machinery: a review, IEEE Access 6 (2018) 66723–66741.
[32] C.-Y. Lin, L. Su, H.-T. Wu, Wave-shape function analysis, J. Fourier Anal. Appl. 24 (2) (2018) 451–505.
[33] L. Lin, Y. Wang, H. Zhou, Iterative filtering as an alternative algorithm for empirical mode decomposition, Adv. Adapt. Data Anal. 1 (04) (2009) 543–560.
[34] Y.-T. Lin, J. Malik, H.-T. Wu, Wave-shape oscillatory model for biomedical time series with applications, arXiv preprint, arXiv:1907.00502, 2019.
[35] S. Mallat, Group invariant scattering, Commun. Pure Appl. Math. 65 (10) (2012) 1331–1398.
[36] M. Materassi, M. Piersanti, G. Consolini, P. Diego, G. D'Angelo, I. Bertello, A. Cicone, Stepping into the equatorward boundary of the auroral oval: preliminary results of multi scale statistical analysis, Ann. Geophys. 62 (4) (2019) 455.
[37] S. Meignen, V. Perrier, A new formulation for empirical mode decomposition based on constrained optimization, IEEE Signal Process. Lett. 14 (12) (2007) 932–935.
[38] I. Mitiche, G. Morison, A. Nesbitt, M. Hughes-Narborough, B.G. Stewart, P. Boreham, Classification of partial discharge signals by combining adaptive local iterative filtering and entropy features, Sensors 18 (2) (2018) 406.
[39] E. Papini, A. Cicone, M. Piersanti, L. Franci, P. Hellinger, S. Landi, A. Verdini, Multidimensional iterative filtering: a new approach for investigating plasma turbulence in numerical simulations, J. Plasma Phys. 86 (5) (2020).
[40] A. Parey, M. El Badaoui, F. Guillet, N. Tandon, Dynamic modelling of spur gear pair and application of empirical mode decomposition-based statistical analysis for early detection of localized tooth defect, J. Sound Vib. 294 (3) (2006) 547–561.
[41] G. Piersanti, M. Piersanti, A. Cicone, P. Canofari, M. Di Domizio, An inquiry into the structure and dynamics of crude oil price using the fast iterative filtering algorithm, Energy Econ. 92 (2020) 104952.
[42] M. Piersanti, M. Materassi, R. Battiston, V. Carbone, A. Cicone, G. D'Angelo, P. Diego, P. Ubertini, Magnetospheric-ionospheric-lithospheric coupling model. 1 observations during the August 5, 2018 Bayan earthquake, Remote Sens. 12 (2020) 3299.
[43] N. Pustelnik, P. Borgnat, P. Flandrin, A multicomponent proximal algorithm for empirical mode decomposition, in: 2012 Proceedings of the 20th European Signal Processing Conference (EUSIPCO), 2012, pp. 1880–1884.
[44] J.L. Flanagan, Speech Analysis Synthesis and Perception, vol. 3, Springer Science & Business Media, 2013.
[45] I.W. Selesnick, Resonance-based signal decomposition: a new sparsity-enabled signal analysis method, Signal Process. 91 (12) (2011) 2793–2809.
[46] R. Sharma, R.B. Pachori, A. Upadhyay, Automatic sleep stages classification based on iterative filtering of electroencephalogram signals, Neural Comput. Appl. 28 (10) (2017) 2959–2978.
[47] L. Spogli, H. Ghobadi, A. Cicone, L. Alfonsi, C. Cesaroni, N. Linty, V. Romano, M. Cafaro, Adaptive phase detrending for gnss scintillation detection: a case study over Antarctica, IEEE Geosci. Remote Sens. Lett. 19 (2022) 1–5.
[48] L. Spogli, M. Piersanti, C. Cesaroni, M. Materassi, A. Cicone, L. Alfonsi, V. Romano, R.G. Ezquer, Role of the external drivers in the occurrence of low-latitude ionospheric scintillation revealed by multi-scale analysis, J. Space Weather Space Clim. 9 (A35) (2019).
[49] A. Stallone, A. Cicone, M. Materassi, New insights and best practices for the successful use of empirical mode decomposition, iterative filtering and derived algorithms, Sci. Rep. 10 (2020) 15161.
[50] J.B. Tary, R.H. Herrera, J. Han, M. van der Baan, Spectral estimation. What is new? What is next?, Rev. Geophys. 52 (4) (2014) 723–749.
[51] M.E. Torres, M.A. Colominas, G. Schlotthauer, P. Flandrin, A complete ensemble empirical mode decomposition with adaptive noise, in: 2011 IEEE International Conference on Acoustics, Speech and Signal Processing (ICASSP), 2011, pp. 4144–4147.
[52] N. Ur Rehman, D.P. Mandic, Filter bank property of multivariate empirical mode decomposition, IEEE Trans. Signal Process. 59 (5) (2011) 2421–2426.
[53] H.-T. Wu, Current state of nonlinear-type time-frequency analysis and applications to high-frequency biomedical signals, arXiv preprint, arXiv:2004.00501, 2020.
[54] Z. Wu, N.E. Huang, Ensemble empirical mode decomposition: a noise-assisted data analysis method, Adv. Adapt. Data Anal. 1 (01) (2009) 1–41.
[55] J.-R. Yeh, J.-S. Shieh, N.E. Huang, Complementary ensemble empirical mode decomposition: a novel noise enhanced data analysis method, Adv. Adapt. Data Anal. 2 (02) (2010) 135–156.
[56] L. Yu, S. Wang, K.K. Lai, Forecasting crude oil price with an emd-based neural network ensemble learning paradigm, Energy Econ. 30 (5) (2008) 2623–2635.
[57] S. Yu, J. Ma, S. Osher, Geometric mode decomposition, Inverse Probl. Imaging 12 (4) (2018) 831.
[58] Z.-G. Yu, V. Anh, Y. Wang, D. Mao, J. Wanliss, Modeling and simulation of the horizontal component of the geomagnetic field by fractional stochastic differential equations in conjunction with empirical mode decomposition, J. Geophys. Res. Space Phys. 115 (A10) (2010).
[59] J. Zheng, J. Cheng, Y. Yang, Partly ensemble empirical mode decomposition: an improved noise-assisted method for eliminating mode mixing, Signal Process. 96 (2014) 362–374.
[60] G. Rilling, P. Flandrin, One or two frequencies? The empirical mode decomposition answers, IEEE Trans. Signal Process. 56 (1) (2007) 85–95.
[61] H.-T. Wu, P. Flandrin, I. Daubechies, One or two frequencies? The synchrosqueezing answers, Adv. Adapt. Data Anal. 3 (2011) 29–39, 01n02.
[62] E. Friis-Christensen, H. Lühr, D. Knudsen, R. Haagmans, Swarm–an Earth observation mission investigating geospace, Adv. Space Res. 41 (1) (2008) 210–216.
[63] N. Linty, A. Minetto, F. Dovis, L. Spogli, Effects of phase scintillation on the GNSS positioning error during the September 2017 storm at Svalbard, Space Weather 16 (9) (2018) 1317–1329.
[64] C.-C. Wu, K. Liou, R.P. Lepping, L. Hutting, The 04–10 September 2017 Sun–Earth connection events: solar flares, coronal mass ejections/magnetic clouds, and geomagnetic storms, Sol. Phys. 294 (8) (2019) 1–19.